Design and Control of an MRI Compatible Series Elastic Actuator

Yusuf Mert Senturk Volkan Patoglu

Abstract— **Bidirectional compatibility requirements with Magnetic Resonance Imaging (MRI) have limited the adaptation of rehabilitation robots for use in MRI machines. In this paper, we present the design and control of a Bowden cable-actuated, MRI-compatible series elastic actuator (SEA) that aims to fulfil the bidirectional compatibility requirements to the maximum extend. The proposed device is built using nonconductive diamagnetic MRI compatible materials, fiber optic sensing units and a Bowden cable based actuation, such that imaging artifacts created under strong magnetic field required for neuro-imaging are minimized. In particular, utilization of Bowden-cable transmission enables the placement of the conventional non-MRI compatible control/signal processing units and electric actuators outside the MRI room. This approach not only helps avoid the MR interference caused by these parts and eliminates safety hazards within the MRI room, but also ensures that the performance of the device is not affected by the strong magnetic field, resulting in ideal bidirectional MRI compatibility. Use of a custom-built fiber optic encoder together with nonconductive leaf spring based elastic element enables torque outputs of the device to be measured and used for closed-loop torque control, rendering the system into a series elastic actuator. The proposed MRI compatible SEA is easily customizable and can be used as the building block of higher degrees of freedom MRI compatible robotic devices. Current prototype is validated to administer continuous torques up to 2 Nm with a torque control bandwidth of 1 Hz and a torque sensing resolution of 0.05 Nm.**

I. Introduction

The population of the world has an aging trend and this trend is even more emphasized in the developed countries. Advanced age is a causal agent of stroke, a major cause of motor function deficiency [1]. An increase in physical dysfunctional problems due to the aging of societies and a shortfall of the amount of manual labor in physiotherapy are natural aftermath of this situation [2]. One approach to address the issue to develop various robotic devices to assist with physical rehabilitation.

Robot assisted rehabilitation devices are becoming invaluable assets for physiotherapy exercises in terms of improving the quality of the rehabilitation sessions by ensuring repeatability and standardization in the movements and decreasing the workload on physiotherapists. Many devices have been successfully integrated into clinics to help meet the increasing demand for treatment of many neurological problems, such as loss of limb function, inability bearing weight, and joint instability.

Y. M. Senturk and V. Patoglu are with the Faculty of Engineering and Natural Sciences, Sabanci University, Istanbul, Turkey. {ymert,vpatoglu}@sabanciuniv.edu

This work is partially supported by Sabanci University and Tubitak Grant 115M698.

With a large variety of robot assisted rehabilitation devices deployed into clinics, ensuring the efficiency of robotic physiotherapy and optimizing the assistance procedure are becoming more pressing issues. Since Magnetic Resonance Imaging (MRI) can be used to monitor the activation of motor cortex during a rehabilitation procedure, MRI studies have high potential to gather decisive information about the efficacy of the treatment protocols [3]. Along these lines, new robot assisted rehabilitation devices compatible with MRI are in high demand. Enabling the brain function to be monitored, these devices can lead to a better understanding the neurological effects of rehabilitation and may lead to development of personalized exercise routines to fulfill the custom needs of each patient.

Development of MRI compatible robotic devices is challenging, since there are strict constraints on the material, sensing and actuation techniques that can be used within an MRI room. In particular, *bidirectional compatibility* must be fulfilled by the device: not only the device should not cause any safety hazards or distort the results of the imaging process by creating additional magnetic fields and emitting radio frequency signals, but also the performance of the device should not be affected by the magnetic field in an MRI room. For instance, all ferromagnetic materials are prohibited, because of the high forces developing on them due to the high magnetic field. Any type of conductive material and electric circuitry are also not preferred, since the eddy currents that develop on these materials cause additional noise that manifests itself as shading, spatial distortion and false positive activation artifacts in the resulting images. Apart from the material constraints, there are also dimensional constraints for the devices that stem from the typically very narrow space available in the bore of MRI machines [4]. Finally, design complexity and cost are of high importance for widespread adaptation of these devices.

This paper introduces the design and control of a low cost, torque controlled, MRI-compatible actuator with ideal bidirectional compatibility.

II. Related Work

MRI compatible rehabilitation devices can be loosely categorized with respect to their actuation scheme as follows:

The devices in the first category are not actuated and aim at measuring the interaction forces or movement patterns of the patients [5]–[7]. Even though the data gathered with these devices are very useful for many applications, the inability of these devices to provide active assistance to patients severely limits their use for evaluating efficacy of robot-assisted rehabilitation procedures.

The devices in the second category are capable of passive impedance modulation through use of electro-rheological fluids [8] or particle jamming techniques [9]. Even though these devices can modulate the impedance that patients physically interact with, they cannot provide active assistance that is required to implement robot-assisted rehabilitation.

The devices in the third category utilize electrostatic motors for MRI-compatible actuation [10]. Use of electrostatic motors is challenging, since they need to be placed certain distance away from the coil of the MRI machine to avoid causing artifacts in the resulting images [11].

The devices with hydraulic actuation constitute the forth category. This approach relies on a master device located outside the MRI room to actuate a mechanical slave linkage inside the room. Since fluid flow near the MRI machine is undesirable as it can interfere with the imaging, a slave device is need [12], [13]. High actuation pressures are required for accurate position control of the system, due to high friction losses of the hydraulic system; however, such high pressures are hard to reach without using metal construction or causing the system to become very bulky. As a result, the complicated master-slave setup and the existence of high valve friction in the hydraulic system limit the use of hydraulic actuation for MRI-compatible force controlled physical human-robot interaction (pHRI).

The devices in the fifth category use pneumatic actuation. Due to compressibility of air and pressure losses in piping/valves, these devices are known to suffer from poor bandwidth and inadequate force control capabilities [14].

The devices in the sixth category rely on ultrasonic motors [15], [16]. While these actuators are MR compatible, the cables and sensors attached to them can cause artifacts in the resulting images. These actuators are not only high cost, but also have high output impedance, which makes them appropriate for motion control applications. Integration of force sensors are needed for their use in pHRI studies. One such solution with ultrasonic motors relies on bronze springs acting as series elastic elements to render the system into a force controlled series elastic actuator [16], [17].

The devices in the seventh category make use of shielded or conventional electric motors that are placed a certain distance away from the MRI machine. Both mechanical linkages [18], [19] and cable-based transmissions [20] have been employed for remote location of the actuators. Since long mechanical linkages introduce undesired elasticity to the system, parallel mechanisms are preferred as the underlying kinematics of these devices, significantly increasing the complexity of the designs. Cable-based transmissions, especially Bowden cable-based power transmissions, are known to introduce friction and non-collocation due to high compliance for long cable lengths. However, coupled with series elastic elements that provide force/torque feedback at the user side, Bowden cable transmissions have been employed by several rehabilitation robots that are not MRI-compatible [21], [22].

In this paper, we present the novel design a low-cost, Bowden cable-actuated series elastic actuator with bidirectional MRI compatibility. Unlike any other closed loop force controlled MR compatible rehabilitation devices in the literature, the design utilizes only nonconductive MRI compatible materials within the MRI room. In particular, a Bowden cable-based transmission and custom fiber optic sensing units are utilized, such that imaging artifacts created under strong magnetic field required for neuro-imaging are minimized. Bowden cable actuation enables for the placement of conventional non-MRI compatible control/signal processing units and electric actuators outside the MRI room (see Figure 1), while polymer leaf spring based series elastic elements and fiber optic encoders enable accurate measurement of interaction torques without causing any interference within the MRI room. The device is torque-controlled through a cascaded force-motion control architecture to enable high fidelity control of interaction torques with the patient. The device is low cost and can be easily customized for use as the building block of higher degrees of freedom MRI compatible robotic devices.

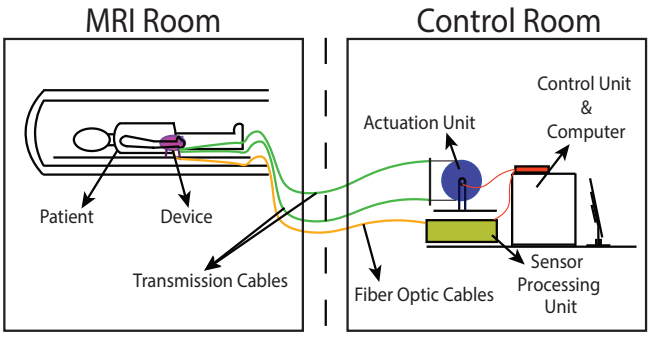

Fig. 1. Schematic representation of remote actuator/controller placement based on Bowden cable-based transmission

III. Design Requirements

In this paper, a design customized for use as a single degree of freedom forearm-wrist rehabilitation device is presented. An imperative design requirement is kinematic compatibility of the device with the human forearm-wrist. Even though the movement of human forearm-wrist is quite complex, simplified kinematics of the human forearm and wrist can be quite faithfully modeled as a 3 DoF kinematic chain that allows supination/pronation of the forearm and flexion/extension and radial/ulnar deviation. Workspace and torque limits of human forearm and wrist of a healthy human are listed in Table I. Since, the torque limits presented for a healthy human is excessively high to perform many activities of daily living (ADL) tasks commonly used for rehabilitation, minimum range of motion and torque limits required to complete ADL tasks are also provided in parenthesis.

To cover the capabilities of human forearm-wrist for ADL tasks, continuous torque output of the device is set to exceed 2 Nm, with a torque control bandwidth of 1 Hz. The workspace of the single degree of freedom device is set to cover $\pm 90^{\circ}$ so that the whole the human range of motion of the forearm-wrist complex can be achieved. A motion bandwidth of at least 5 Hz is desired within the human range so that the device is a few times faster than motion bandwidths commonly used for rehabilitation exercises.

TABLE I

WORKSPACE AND TORQUE LIMITS OF FOREARM AND WRIST [23]

Joint	Human Isometric Strength	Human Joint Workspace Limits
Forearm Supination/Pronation	9.1 Nm (0.02 Nm)	Supination: 86° (86°) Pronation: 71° (71°)
Wrist Flexion/Extension	19.8 Nm (0.5 Nm)	Flexion: 73° (45°) Extension: 71° (50°)
Wrist Radial/Ulnar Deviation	20.8 Nm (0.5 Nm)	Radial Dev.: 19° (19°) Ulnar Dev.: 40° (40°)

Ideal bidirectional MRI compatibility is taken the other imperative design criterion, such that neither the device causes artifacts in the resulting images, not the strong magnetic fields interfere with the functioning of the device. To achieve ideal bidirectional compatibility, no MR incompatible materials are allowed within the MRI room; actuation and sensor processing units are located outside the MRI room and only MR compatible parts are used for both data and power transmission.

Small device volume is considered as a primary design requirement, while a robust design and low cost are taken as secondary design requirements.

IV. DESIGN AND IMPLEMENTATION

A. Mechanical Construction

The actuator body consists of three main plastic parts: support, exterior shell and output shaft, as presented in Figure 2. Support is the grounded part, on which whole device is assembled. The first part to connect to the support is the support shaft. Other rotating bodies are mounted on this support shaft with dual fully ceramic bearings that have lower friction and elasticity in comparison to their metal counterparts. The exterior shell is actuated by tear-resistant Dyneema ropes going through plastic case segments and the ropes are coiled around to the exterior shell inside custom made grooves. The ropes exit the grooves tangentially along opposite directions perpendicular to the axis of rotation, so that the shear for applied to support shaft can be kept minimal at all times. The torque generated due to the distance between the ropes is supported by the double bearings on the support shaft. The output shaft is connected to the exterior shell through compliant plastic leaf spring elements.

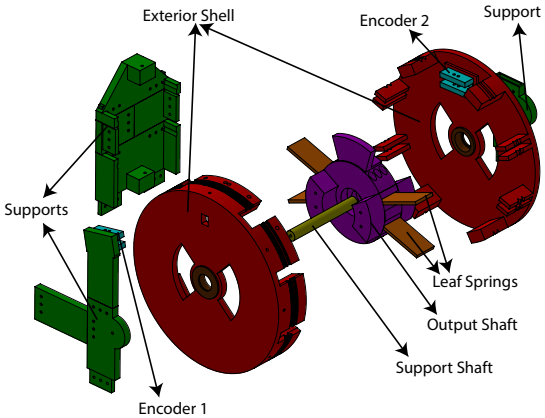

Fig. 2. An exploded view of the MRI-compatible SEA

There are two encoders on the device: one mounted on the support to measure the angular displacement and velocity of the exterior shell and another mounted between the output shaft and the exterior shell parallel to the compliant elements to measuring it the deflection of the output shaft with respect to the exterior shell. The exterior shell is designed to enable the output shaft to rotate by deflecting the leaf springs, while hard stops are implemented not to exceed predetermined deflection amounts. Figure 3 presents a schematic representation of the deflections of the series elastic element and the deflection measurements.

Figure 4 presents CAD models including the implementation details of the design. In the current prototype the exterior case, output shaft and the support are 3-D printed from ABS polymer, which is known to be compatible with MR environment [24]. The compliant elements are cut from Garolite sheets that are guaranteed not to interfere with radio frequency signals and insulate electricity. The encoder cases are made of polyoxymethylene (Delrin) and the fiber optic cables are metal free only having cable core, jacket and the ceramic ferrule.

B. Series Elastic Element

Many optical force sensors developed for MR environment suffer from the cross-coupling of forces and moments on the sensor body due to the dependence of force readings on deflections in the body of the sensor and inability to separate the unidirectional deflections caused by specific forces and torques, as pointed out in [25]. Use of leaf springs as compliant elements is advantageous, since due to their geometry in the form of a rectangular plate, leaf springs display high bending, torsion and elongation resistance to the forces and torques in the directions other than the desired direction of deflection. Only the bending torques along the direction of the shaft can cause significant deflections in the these springs as depicted in Figure 3. The deflections caused by such torques are measured by fiber optic encoders near the outer diameter of the exterior shell such that the displacements are large enough to estimate interaction torques with sufficient resolution.

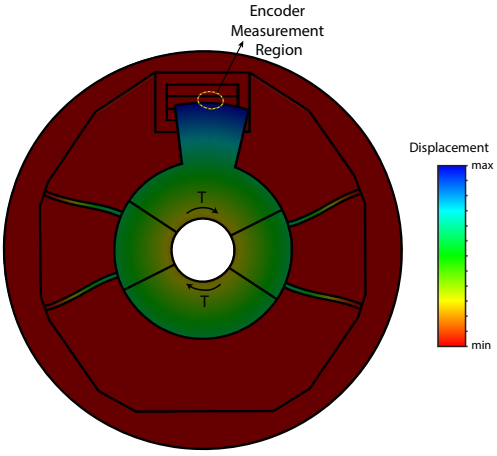

Fig. 3. Schematic representation of the deflections of the series elastic element and deflection measurements

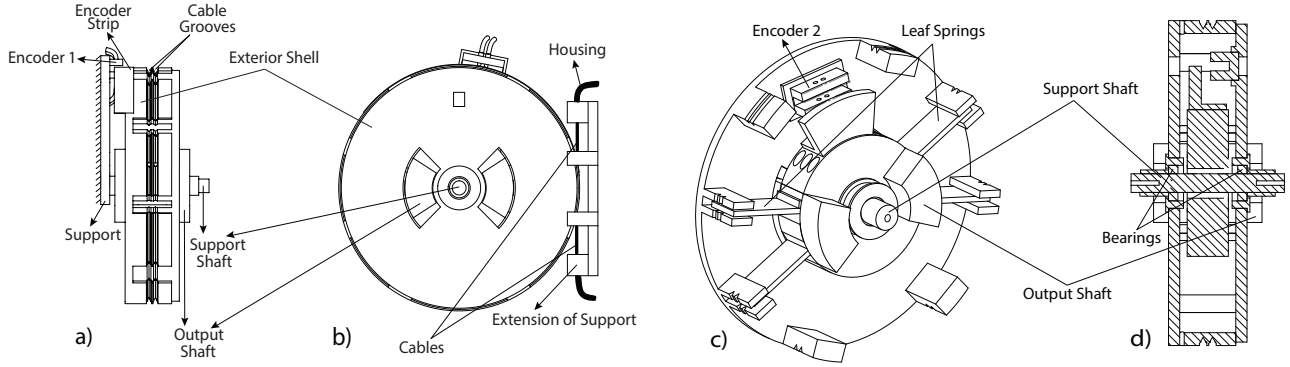

Fig. 4. a) Side-view: Cable grooves and the strip of Encoder-1 b) Front-view: Actuation via Bowden Cables c) Inside-view: Encoder-2 (without encoder strip for better visualization) and leaf springs d) Cross-sectional view: Bearings and support shaft

C. MRI Compatible Fiber Optic Encoder

To implement series elastic actuation, rotations of the external shell and the deflections of the leaf springs need to be measured. Standard optical encoders cannot be utilized inside MRI machine, since metal parts and conductive wires in these sensors lead to image artifacts. Neither magnetic encoders is an option.

To avoid any conductive materials or wiring inside the MRI room, custom-built fiber optic encoders are developed. Since fiber optics transfer data through light signals, very high communication rates can be easily archived, while MR incompatible sensor processing units can be placed outside the MRI room. Furthermore, not only fiber optic components are wide-spread and low-cost; these components typically feature plastic construction.

The custom-built fiber optic encoder, shown in Figure 5, possesses the same working principles of a conventional quadrature encoder. Signal processing of the encoder signals is performed using similar integrated circuit elements. The sensor system consists of a transmitter (source), a receiver (sink), light transferring fiber optic cables, an encoder case, an encoder strip and signal processing elements. Fiber optic cables are chosen to have straight tip/physical contact connections and a core diameter of 62.5 μm. These cables are the most prevalent type for use in the short distance communication and support signal frequencies over 100 MHz, which is about hundred times faster than the frequency needed to read the encoder strip moving in the vicinity of human motion bandwidth. The transmitter and the receiver are commercially available low cost components and support data communications up to 125 MHz. The encoder strip is chosen to have appropriate line count per length, to ensure compatibility with the core diameter of the cable. In particular, the distance between lines on the encoder strip should be smaller than the core diameter of the fiber optic cable; otherwise, the measurements may be erroneous.

The case of the encoder is manufactured using a micro CNC machine. During fabrication, the opposing pair of holes for the ferrules of the fiber optic cables must be drilled simultaneously in order to ensure the alignment of the light beam. While designing the distance between the pairs of holes, the distance l between the lines of the encoder strip

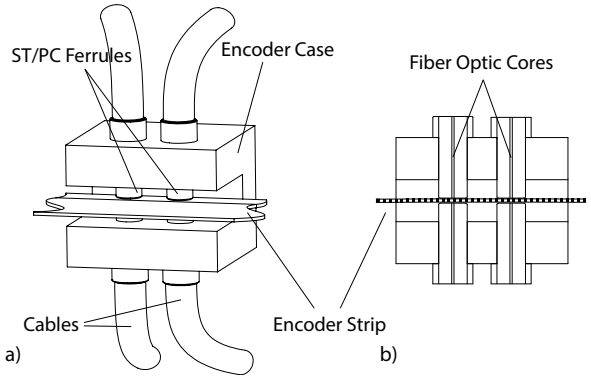

Fig. 5. a) Encoder assembly b) Cross-section of the encoder

should taken into consideration. In particular, the distance can be chosen as $2k \pm 1/2$ multiple of l, where k is a positive integer. Such an arrangement ensures that the A and B signals of the encoder are $\pm\pi/2$ out of phase. Proper phase alignment is especially critical for performing accurate velocity estimations using the encoder readings under quadrature decoding. Current encoder prototype is designed to work with 250 to 300 line per inch encoder strips. Encoder resolution can be further increased by decreasing the thickness of the fiber optic cable.

D. Sensor Processing Unit

The sensor processing unit is placed outside the MRI room, since sensor data can be communicated over long distances through fiber optics. The signals from the encoders are quite noisy, due to the use of the fiber optic communication elements for open air light transmission through the encoder strip in order to create appropriate encoder signals. The signals contain extensive high frequency noise, especially during rise and fall instances, since complex, oscillatory and high frequency diffraction patterns of light are formed at the instants, when the transitions from transparent strip line to opaque line (or vice versa) occur. The effect of this noise is bounded by a single encoder count for position readings, since rise and falls due to noise occur sequentially. Even though the effect of the noise on position measurement is negligible, its effect on velocity estimations is more extensive.

To reduce the noise, signal processing is implemented in

hardware by first downsizing the amplitude of the noise using a RC circuit as a low pass filter and then implementing a Schmitt trigger using a rail-to-rail op-amp. Even though a fast slew rate of 3V/μs can be achieved, rises and falls of the processed signal are not fast enough for velocity estimations through windowing. In particular, when the encoder reading module detects that the signal is rising, the velocity is increased. Slow rise can cause the velocity to be increased at multiple time steps instead of only once. To address this issue, a high slew rate comparator with 5V/80ns rise time is employed as the last step of signal processing. Figure 6 depicts a schematic representation of the signal processing scheme for the fiber optic encoders.

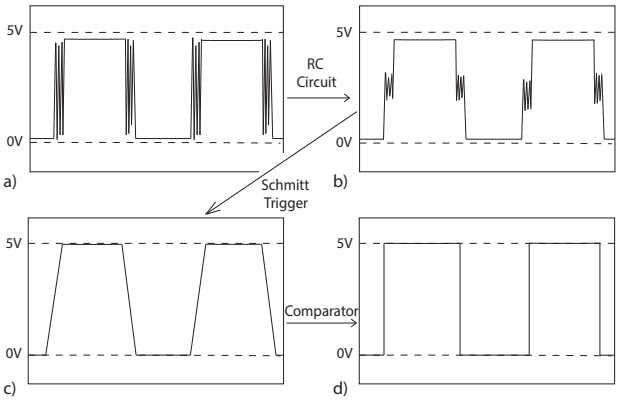

Fig. 6. Schematic representation of the encoder signal processing scheme: a) RC circuit low-pass filter, b) Schmitt trigger, and c) comparator

E. Actuation Unit

The actuation unit is located outside the MRI room along with the sensing and control equipment, since long Bowden cables can be used to transfer power from the motors to the MRI compatible device. Decoupling the actuation unit that weighs more than 15 kg from the MRI compatible part not only ensures bidirectional compatibility, but also reduces the size and weight of the device to be placed in the MRI room unit to a mere 0.3 kg.

In the current prototype, presented in Figure 7, the actuator is selected as a 200 Watt, coreless, rare magnet DC motor coupled to a harmonic drive with 1:50 gear ratio. A large pulley is attached to the actuator and this arrangement provides a cumulative 1:223 transmission ratio between the external shell of the MRI compatible device and the DC motor. The Bowden cable transmission consist of tear-resistant Dyneema ropes and plastic shields of 1.5 m length.

V. Series Elastic Actuation and Torque Control

The MRI compatible actuator is powered through a Bowden cable-driven SEA, similar to those of [21], [22]. Bowden cable-drive not only ensures bidirectional MRI compatibility by enabling the controller and actuator units be conveniently placed outside the MRI room, but also ensures that the device possesses a lightweight and portable design with significantly low volume to fit the narrow bore of MRI machines, while simultaneously providing large enough actuation torques required to assist human forearm-wrist.

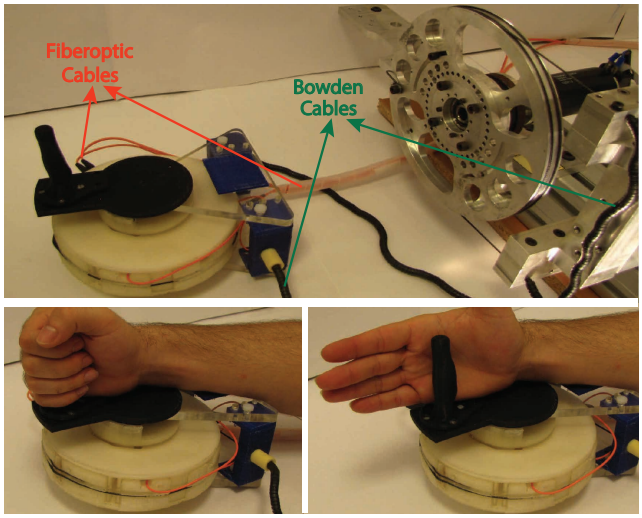

Fig. 7. Current prototype of the MRI-compatible SEA. Upper figure shows the device with its remote actuation unit, while the lower figures present interaction with a user.

The high friction in Bowden cables and harmonic drive reduction units results in a passively non-backdrivable power transmission system. To ensure high fidelity torque control for assisting patients while simultaneously reducing the output impedance of the system for safety, series elasticity (compliant elements) are intentionally introduced between the Bowden cable-driven exterior shell and the output link. The deliberate introduction of compliance between the Bowden-cable driven actuation unit and the patient-attached link transforms the passively non-backdrivable actuator into a series elastic one, where the compliant element is used as the torque sensing unit by measuring its deflections.

Since SEA features orders of magnitude higher compliance of its sensing unit compared to a conventional torque sensor, much higher torque controller gains can be used for its robust torque control, without endangering the inherent stability limits induced by sensor-actuator non-collocation. As controllers with higher gains are more responsive and robust against undesired disturbances, low cost transmission and actuation units, possibly with parasitic dynamics such as friction and stiction, can be employed in the design of SEAs to achieve high fidelity torque control. In particular, with SEA, precise control of the torques can be achieved through robust *motion* control of the deflection of the compliant coupling element. Furthermore, since high precision actuators/power transmission elements or torque sensors are not necessitated, the device costs can also be kept significantly lower compared to conventional torque controlled devices.

SEA possesses high-fidelity torque control and active backdrivability within its control bandwidth, while also featuring passive elasticity for excitations above this bandwidth, ensuring safety and robustness throughout the whole frequency spectrum, including hard impacts that may take place [22], [26].

A real-time cascaded controller is implemented for control of MRI compatible SEA as shown in Figure 8. The cascaded controller consists of an inner robust velocity control loop

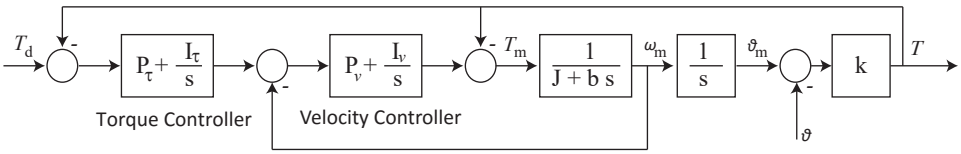

Fig. 8. Cascaded SEA controller architecture with inner velocity control loop and outer torque control loop

and and outer torque control loop. The inner motion control loop implemented on the motor controller at 10 kHz compensates for imperfections, such as friction and stiction, rendering the system into an ideal velocity source. The outer torque control loop is implemented at 1 kHz such that the effective interaction torques can be set to appropriate values.

VI. Experimental Verification

A. Stiffness of the Series Elastic Element

Dynamic Mechanical Analysis (DMA) is performed on the Garolite leaf spring with a three point bending test at different frequencies around 1 Hz for a range of temperatures. No change in the measured properties is observed within the 20°–50° temperature range. Mechanical properties of the leaf spring, such as elastic modulus of the material, are derived from the force and displacement data gathered by this experiment using the Euler-Bernoulli beam equation. These mechanical properties are then used to perform finite element analysis (FEA) of the system to determine the deflections of the compliant element at the encoder measurement region under load torques applied to the output shaft. Figure 9 presents the data collected from these FEA results together with a linear least squares fit (R^2 = 0.9999).

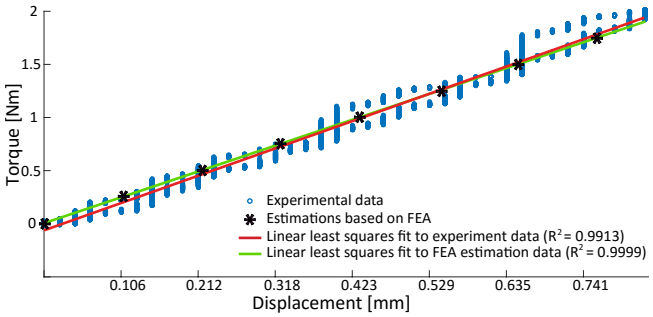

Fig. 9. Data collected during the experiments, together with FEA estimations and linear least squares curve fits, characterizing the stiffness of the series elastic element

Experimental characterization of the series elastic element is also performed using a force sensor rigidly attached to the output shaft (See Figure 7, left). Sinusoidal torque inputs at different frequencies up to 1 Hz are administered to the system over a period of time corresponding to 30 cycles, during which encoder measurements are recorded. Displacement and torque measurements from these experiments are plotted in Figure 9, together with a linear least squares fit (R^2 = 0.9913). No hysteresis has been observed up to 1 Hz, the required upper limit of the torque bandwidth. The stiffness estimates, taken as the slope of least square line fits, are observed to be a good match between the FEA analysis and experimental data, with less than 5% error.

B. Torque Tracking Performance

The static and dynamic torque control performance of the MRI compatible SEA is presented in Figures 10 and 11. In Figure 10, the set point torque control results are reported for three reference torque values: 1 Nm, 2 Nm and 3 Nm. The steady state torque error for these three references are within the torque sensing resolution, while rise and settling times are less than 0.25 s and 0.6 s, respectively.

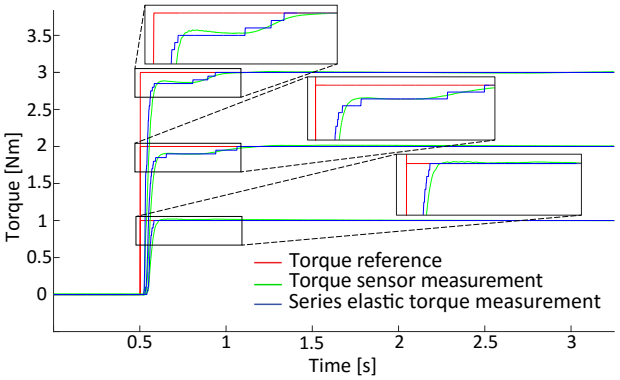

Fig. 10. Set-point torque control performance of MRI compatible SEA

Figure 11 depicts the torque tracking performance of the SEA for a sinusoidal reference signal at 1 Hz with 2 Nm peak-to-peak amplitude. The percent RMS error for this tracking experiment is characterized to stay under 4%.

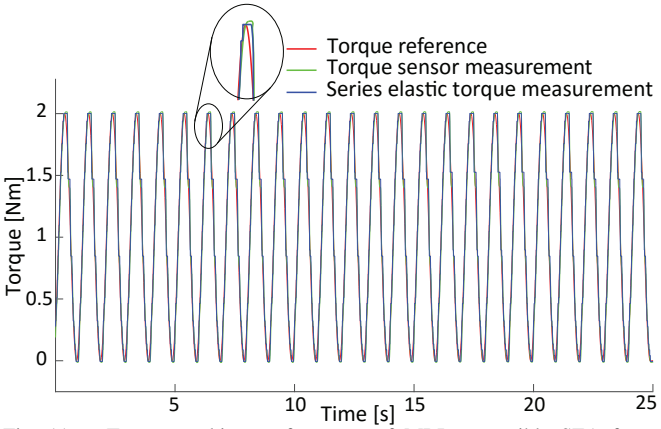

Fig. 11. Torque tracking performance of MRI compatible SEA for a sinusoidal reference signal at 1 Hz with 2 Nm peak-to-peak amplitude

VII. Discussion and Conclusions

The design and control of a Bowden cable-actuated, MRI-compatible SEA with ideal bidirectional compatibility are presented. Since the device is built using nonconductive MRI compatible materials, fiber optic sensing units and Bowden cable-based actuation, it can, not only minimize any interference that can cause imaging artifacts during neuro-imaging, but also ensure that device performance is not affected by strong magnetic fields.

In particular, [27] evaluates compatibility of a device with MR environment considering five criteria: device movement, device heating, induced electrical currents, image distortion and device operation. Device movement is caused by forces due to the presence of ferromagnetic materials in an MRI machine. Since the proposed device consists of diamagnetic materials, such forces are not possible. Device heating stems from electromotive forces on conductive elements. Since all materials in the proposed design are classified as insulators, there is no possibility of such heating that may cause operational dysfunctions and safety hazards. Furthermore, since no conductive materials or circuitry is used inside the MRI room, there is also no risk of inducing currents that can create artifacts on the image. The proposed device does not distort the magnetic field outside of its volume, since no currents are induced on it. Finally, the device operation is not affected by the MRI procedure, thanks to its Bowden cable-based power and fiber optic data transmission.

Current prototype is a single degree of freedom actuator built to administer forearm-wrist exercises within an MRI machine. However, the design is easily customizable and can be used as the building block of higher degrees of freedom MRI compatible robotic devices. In particular, stiffness of the series elastic element can be customized by simply changing the dimensions of the leaf springs, the resolution of the fiber optic encoders can be adjusted by employing fiber optic cables with smaller core diameters together with higher resolution encoder strips, while torque output of the device can be adjusted by utilizing more powerful motors.

Ongoing studies include experimental verification of the MRI compatibility and use of the device as part of neuro-imaging studies.

REFERENCES

[1] P. A. Wolf, R. B. D'Agostino, A. J. Belanger, and W. B. Kannel, "Probability of stroke: a risk profile from the framingham study.," *Stroke*, vol. 22, no. 3, pp. 312–318, 1991.

[2] W. S. Lutz, Wolfgang and S. Scherbov, "The coming acceleration of global population ageing," in *Nature, 451(7179)*, pp. 716–719, 2008.

[3] Y. Dong, B. H. Dobkin, S. Y. Cen, A. D. Wu, and C. J. Winstein, "Motor cortex activation during treatment may predict therapeutic gains in paretic hand function after stroke," *Stroke*, vol. 37, no. 6, pp. 1552–1555, 2006.

[4] R. Gassert, E. Burdet, and K. Chinzei, "Opportunities and challenges in MR-compatible robotics," *IEEE Engineering in Medicine and Biology Magazine*, vol. 27, no. 3, pp. 15–22, 2008.

[5] J. Hidler, T. Hodics, B. Xu, B. Dobkin, and L. G. Cohen, "MR compatible force sensing system for real-time monitoring of wrist moments during fMRI testing," *Journal of neuroscience methods*, vol. 155, no. 2, pp. 300–307, 2006.

[6] J. M. Newton, Y. Dong, J. Hidler, P. Plummer-D'Amato, J. Marehbian, R. M. Albistegui-DuBois, R. P. Woods, and B. H. Dobkin, "Reliable assessment of lower limb motor representations with fMRI: use of a novel MR compatible device for real-time monitoring of ankle, knee and hip torques," *Neuroimage*, vol. 43, no. 1, pp. 136–146, 2008.

[7] J. P. Mehta, M. D. Verber, J. A. Wieser, B. D. Schmit, and S. M. Schindler-Ivens, "A novel technique for examining human brain activity associated with pedaling using fMRI," *Journal of neuroscience methods*, vol. 179, no. 2, pp. 230–239, 2009.

[8] S. Menon, A. A. Stanley, J. Zhu, A. M. Okamura, and O. Khatib, "Mapping stiffness perception in the brain with an fMRI-compatible particle-jamming haptic interface," in *Annual International Conference of the IEEE Engineering in Medicine and Biology Society*, pp. 2051–2056, 2014.

[9] A. Khanicheh, D. Mintzopoulos, B. Weinberg, A. A. Tzika, and C. Mavroidis, "Evaluation of electrorheological fluid dampers for applications at 3-T MRI environment," *IEEE/ASME Transactions on Mechatronics*, vol. 13, no. 3, pp. 286–294, 2008.

[10] M. Hara, G. Matthey, A. Yamamoto, D. Chapuis, R. Gassert, H. Bleuler, and T. Higuchi, "Development of a 2-dof electrostatic haptic joystick for MRI/fMRI applications," in *IEEE International Conference on Robotics and Automation*, pp. 1479–1484, 2009.

[11] A. Yamamoto, K. Ichiyanagi, T. Higuchi, H. Imamizu, R. Gassert, M. Ingold, L. Sache, and H. Bleuler, "Evaluation of MR-compatibility of electrostatic linear motor," in *IEEE International Conference on Robotics and Automation*, pp. 3658–3663, 2005.

[12] R. Gassert, R. Moser, E. Burdet, and H. Bleuler, "MRI/fMRI-compatible robotic system with force feedback for interaction with human motion," *IEEE/ASME Transactions on Mechatronics*, vol. 11, no. 2, p. 216, 2006.

[13] R. Gassert, L. Dovat, O. Lambercy, Y. Ruffieux, D. Chapuis, G. Ganesh, E. Burdet, and H. Bleuler, "A 2-DOF fMRI compatible haptic interface to investigate the neural control of arm movements," in *IEEE International Conference on Robotics and Automation*, pp. 3825–3831, 2006.

[14] N. Yu, C. Hollnagel, A. Blickenstorfer, S. S. Kollias, and R. Riener, "Comparison of MRI-compatible mechatronic systems with hydrodynamic and pneumatic actuation," *IEEE/ASME Transactions on Mechatronics*, vol. 13, no. 3, pp. 268–277, 2008.

[15] M. A. Ergin, M. Kuhne, A. Thielscher, and A. Peer, "Design of a new MR-compatible haptic interface with six actuated degrees of freedom," in *IEEE RAS & EMBS International Conference on Biomedical Robotics and Biomechatronics*, pp. 293–300, 2014.

[16] F. Sergi, A. C. Erwin, and M. K. O'Malley, "Interaction control capabilities of an MR-compatible compliant actuator for wrist sensorimotor protocols during fMRI," *IEEE/ASME Transactions on Mechatronics*, vol. 20, no. 6, pp. 2678–2690, 2015.

[17] F. Sergi, A. Erwin, B. Cera, and M. K. O'Malley, "Compliant force-feedback actuation for accurate robot-mediated sensorimotor interaction protocols during fMRI," in *IEEE RAS & EMBS International Conference on Biomedical Robotics and Biomechatronics*, pp. 1057–1062, 2014.

[18] S. Li, A. Frisoli, L. Borelli, M. Bergamasco, M. Raabe, and M. W. Greenlee, "Design of a new fMRI compatible haptic interface," in *World Haptics*, pp. 535–540, 2009.

[19] S. Menon, H. Ganti, and O. Khatib, "Using haptic fMRI to enable interactive motor neuroimaging experiments," in *Experimental Robotics*, pp. 89–103, Springer, 2016.

[20] U. Spaelter, D. Chapuis, R. Gassert, R. Moser, and H. Bleuler, "A versatile MRI/fMRI compatible spherical 2-dof haptic interface," in *IEEE/RAS-EMBS International Conference on Biomedical Robotics and Biomechatronics*, pp. 727–732, IEEE, 2006.

[21] J. F. Veneman, R. Ekkelenkamp, R. Kruidhof, F. C. van der Helm, and H. van der Kooij, "A series elastic-and bowden-cable-based actuation system for use as torque actuator in exoskeleton-type robots," *The international journal of robotics research*, vol. 25, no. 3, pp. 261–281, 2006.

[22] A. Erdogan, B. Celebi, A. C. Satici, and V. Patoglu, "AssistOn-Ankle: a reconfigurable ankle exoskeleton with series-elastic actuation," *Autonomous Robots*, pp. 1–16.

[23] N. Tsagarakis, D. G. Caldwell, and G. A. Medrano-Cerda, "A 7-DoF pneumatic muscle actuator powered exoskeleton," in *IEEE International Symposium on Robot and Human Interactive Communication*, pp. 327–333, 1999.

[24] S. Hao, A. Camilo, G. A. Cole, H. Nobuhiko, C. M. Tempany, and G. S. Fischer, "High-field MRI-compatible needle placement robot for prostate interventions," *Studies in health technology and informatics*, vol. 163, p. 623, 2011.

[25] U. Tan, B. Yang, R. Gullapalli, J. P. Desai, *et al.*, "Triaxial MRI-compatible fiber-optic force sensor," *IEEE Transactions on Robotics*, vol. 27, no. 1, pp. 65–74, 2011.

[26] J. Sensinger and R. Weir, "Improvements to series elastic actuators," in *IEEE/ASME International Conference on Mechatronic and Embedded Systems and Applications*, pp. 1–7, 2006.

[27] B. A. Schueler, T. B. Parrish, J.-C. Lin, B. E. Hammer, B. J. Pangrle, E. R. Ritenour, J. Kucharczyk, and C. L. Truwit, "MRI compatibility and visibility assessment of implantable medical devices," *Journal of magnetic resonance imaging*, vol. 9, no. 4, pp. 596–603, 1999.